Peer-reviewed version available at *Materials* **2018**, *11*, 351; doi:10.3390/ma11030351

Optical properties of complex plasmonic materials studied with extended effective medium theories combined with RCWA

Elie Nadal[1,2], *Noémi Barros*[1,2], *Hervé Glénat*[2], *Hamid Kachakachi*[1,2]

[1] University of Perpignan Via Domitia (UPVD), 52 Avenue Paul Alduy, 66100 Perpignan, France

[2] PROMES, CNRS (UPR8521), Rambla de la thermodynamique, 66100, Perpignan, France.

Corresponding author: elie.nadal@univ-perp.fr

KEYWORDS: gold nanoparticles, plasmon, nanocomposites, laser interferometry, Maxwell-Garnett theory, gratings, diffraction, RCWA.

ABSTRACT: In this study we fabricate gold nanocomposites and model their optical properties. The nanocomposites are either homogeneous films or gratings containing gold nanoparticles embedded in a polymer matrix. The samples are fabricated using a recently developed technique making use of laser interferometry. The gratings present original plasmon-enhanced diffraction properties. In this work, we develop a new approach to model the optical properties of our composites. We combine the extended Maxwell-Garnett model of effective media with the Rigorous Coupled Wave Analysis (RCWA) method and compute both the absorption spectra and the diffraction efficiency spectra of the gratings. We show that such a semi-analytical approach allows us to reproduce the original plasmonic features of the composites and can give us entails about their inner structure. Such approach could be a simple and efficient tool to study complex micro-structured system based on plasmonic components, such as metamaterials.

Peer-reviewed version available at Materials 2018, 11, 351; doi:10.3390/ma11030351

Introduction

Complex plasmonic systems, and in particular plasmonic nanocomposites, have emerged as promising materials for numerous applications in photonics [1–3], photovoltaics [4–7] and in environmental issues such as water remediation [8–10] or hydrogen production through water splitting [11–13]. Indeed, due to their plasmonic features, these systems exhibit novel optical as well as electrical properties. The control of these features, with the purpose to design functional materials or devices with tailored functionalities, often requires an organization of the metallic nanostructures into specific arrangements [14]. For instance, in photonics, the design of metamaterials, defined as exotic materials producing non-natural optical properties, mostly relies on the ability to create complex and regular 3D composite superlattices [3,15,16]. The insertion of plasmonic nanostructures in organic solar cells has also been demonstrated as an efficient way to improve the conversion efficiency of these devices. Once again, the different scenarios used to enhance the optical properties of the system strongly rely on the ability to precisely insert the metallic particles, acting as absorbers or diffusers, inside the device structure [4,17]. Finally, very recently, plasmonic circuits based on well-defined nano and micro metallic patterns have been proposed as a new benchmark to build optical computers [18,19].
The optical properties of such organized plasmonic materials are complex and difficult to describe theoretically since both the intrinsic properties of the nanostructures and the long-range organization must be taken into account [20]. Generally, two main approaches are used to calculate the optical properties of plasmonic systems. The first approach consists in solving the Maxwell equations for a few nanostructures described explicitly. This approach relies on exact numerical simulations which require high computer resources, among which the most commonly used are Discrete Dipole Approximation (DDA) [21,22], Finite Difference Time Domain (FDTD) [23] and Boundary Element Method (BEM) [24,25]. These methods are very efficient for quite precisely computing both the optical spectra and the electric field maps of any nanostructure placed in a given medium. However, the computing time rapidly increases with the size of the system, thus limiting these methods to the study of very small nanoparticle assemblies [26]. The second approach is analytical and relies on the effective medium theories [27], the most famous being the Maxwell-Garnett (MG) theory [28]. Unlike the previous approach, the effective-medium phenomenological theories make it possible to tackle nanocomposites consisting of a large number of nanostructures. However, they proceed by averaging over size, shape and orientation distribution and thus usually smooth out the intrinsic features of the nanoparticles.

In the present work, we propose a method for describing the optical properties of plasmonic systems with a multi-scale spatial organization consisting of ensembles of plasmonic nanostructures regularly distributed at the micrometer range. For that, we adopt an intermediate approach combining the semi-analytical MG theory and the so-called numerical method Rigorous Coupled Wave Analysis (RCWA) [29,30]. As a benchmark, we use gold nanoparticle gratings (GNGs) fabricated by laser interference patterning. In these systems, assemblies of nanoparticles are distributed in a polymer matrix forming 1D gratings with a period of 2 micrometers, see Fig. 1(a).

Preprints (www.preprints.org) | NOT PEER-REVIEWED | Posted: 5 February 2018 doi:10.20944/preprints201802.0039.v1

Peer-reviewed version available at Materials 2018, 11, 351; doi:10.3390/ma11030351

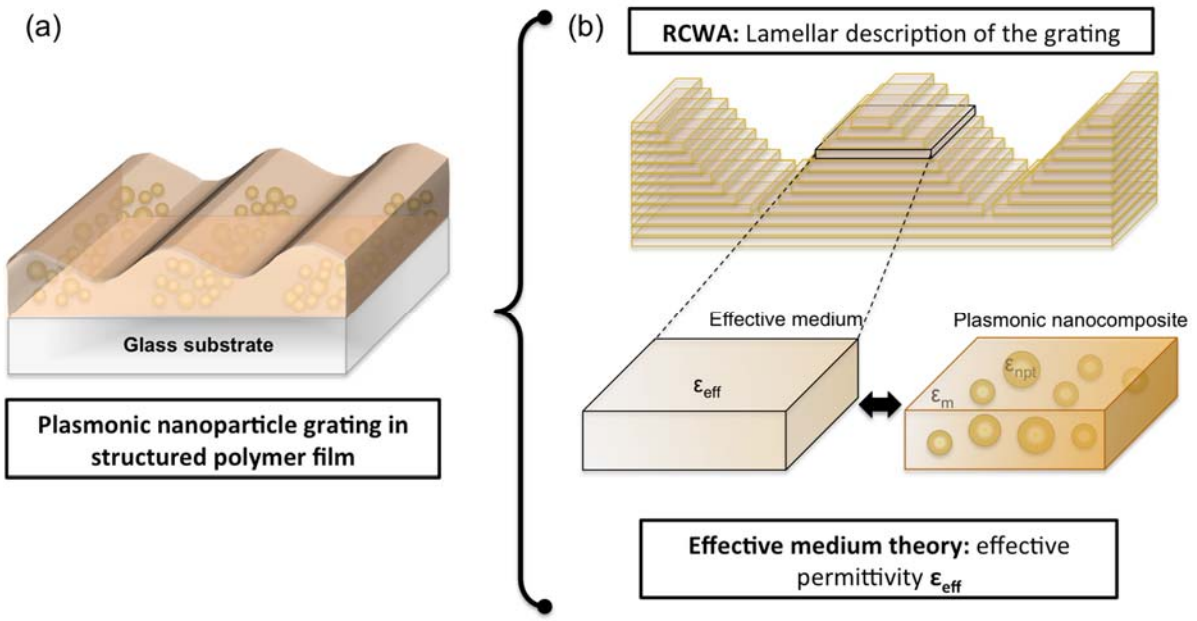

Figure 1: (a) Gold nanoparticle gratings in polymer thin films and (b) modeling of the system by combining the RCWA and the effective medium theory.

We prepare several gratings with a variable gold/polymer ratio and study the effect of the gold volume fraction on the optical properties. The periodic nature of the system is dealt with the help of RCWA, which makes use of a stratified description of the composites, each stratum being described by its dielectric permittivity. The plasmonic properties of the nanocomposites are then introduced by replacing the dielectric permittivity of each stratum by an effective permittivity computed using the extended MG model. The modeling procedure is sketched in Fig. 1(b). This method allows us to compute the optical properties of the film and it particular the diffraction, the plasmonic nanostructures being described implicitly.

Materials and methods

Now, we briefly present the fabrication approach used to synthesize the GNGs. The detailed fabrication procedure is given in Ref. 31 and is summarized in Section A, Fig. S1 of the Supplementary Material (SM). We prepare 3 gratings with gold/polymer ratios of 3w%, 5w% and 10w%. A polyvinyl alcohol (PVA) solution containing the appropriate amount of gold precursors is spin-coated on glass substrates. The films thus obtained are homogeneously doped with gold ions. Then, a Mach Zehnder interferometer is used to irradiate the sample with an interference pattern, thus performing a spatially controlled photo-reduction of the gold salt. Finally, nanoparticle growth is triggered by annealing the samples. It is observed that the nanoparticles are mainly formed in the irradiated areas (bright fringes of the interference pattern), and induce the deformation of the polymer film, leading to the appearance of sinusoidal surface relief gratings. As a comparison, another set of samples is prepared using the same procedure except for the irradiation part, which is performed with a homogeneous Gaussian beam instead of the interference pattern. Consequently, at the end of the procedure, the samples thus irradiated are loaded with gold

Preprints (www.preprints.org) | NOT PEER-REVIEWED | Posted: 5 February 2018 doi:10.20944/preprints201802.0039.v1

Peer-reviewed version available at Materials 2018, 11, 351; doi:10.3390/ma11030351

nanoparticles homogeneously distributed in the films. This second set of samples will be denoted as homogeneous films (HFs).

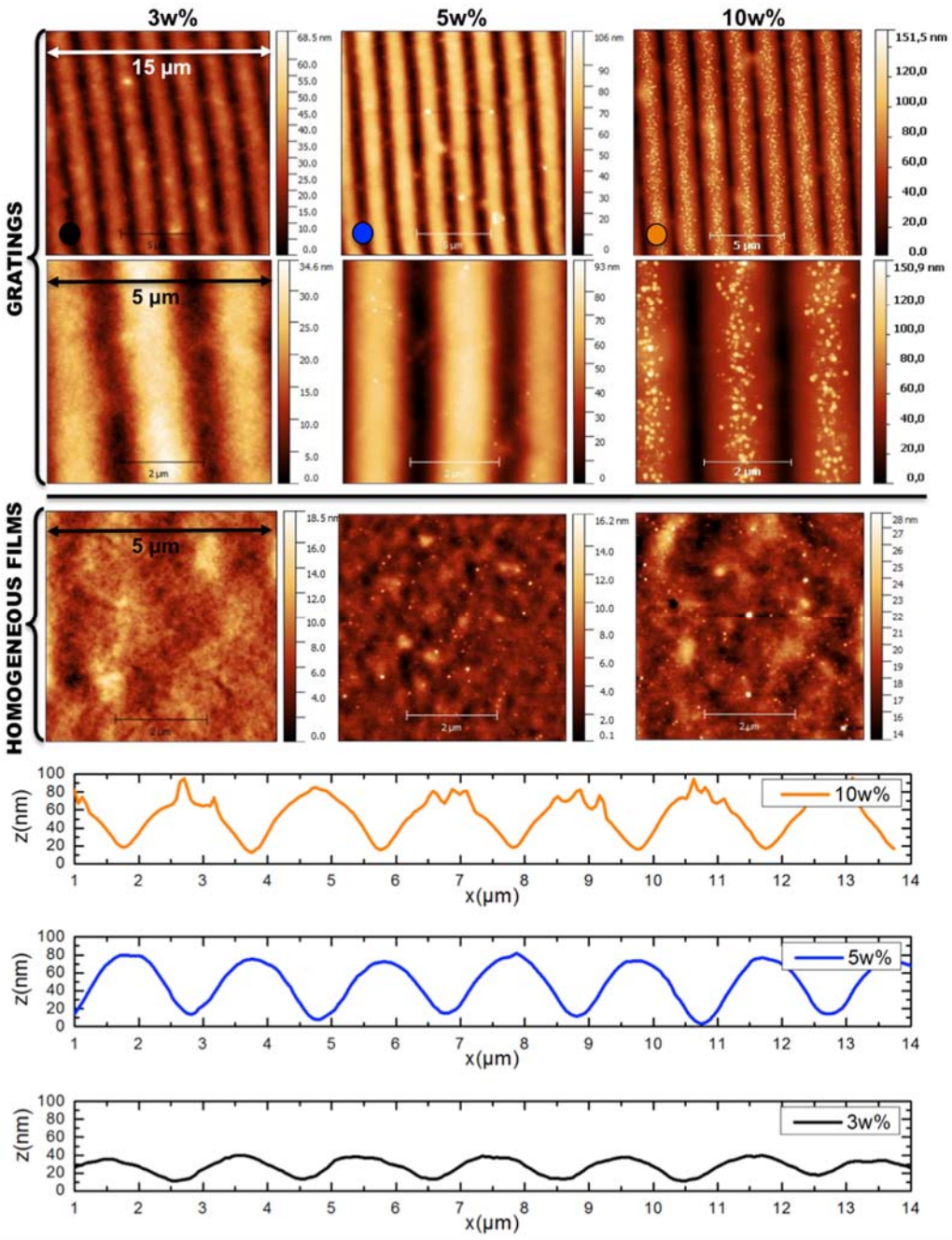

Figure 2: AFM images of the different GNGs (upper panel) and the different HFs (middle panel) with gold/polymer ratio of 3w%, 5w% and 10w%. The surface profiles of the gratings are shown in the lower panel.

The obtained films have an average thickness of 800 nm. AFM images of the various GNGs and the HFs with gold/polymer ratio of 3w%, 5w% and 10w%, along with the surface profile of the gratings are given in Fig.2. As can be seen, the height of the surface modulation of the gratings increases with the gold concentration, going from 25 nm to 80 nm, whereas the HFs remain flat at all concentrations. For low gold ratios, the nanoparticles are embedded in the films, but become clearly visible at the film surfaces as the gold concentration increases. In

Preprints (www.preprints.org) | NOT PEER-REVIEWED | Posted: 5 February 2018 doi:10.20944/preprints201802.0039.v1

Peer-reviewed version available at Materials 2018, 11, 351; doi:10.3390/ma11030351

the case of the grating with 10w% gold, the nanoparticles start emerging at the top of the grating crests, which results in an uneven surface profile.
Absorption spectra are measured on all samples by using standard spectroscopic techniques. A dedicated setup [31] is used to measure the diffraction efficiency of the gratings, details are given in the SM (Section A, Fig. S2).

Analytical and numerical models

In this section, we first introduce our approach for computing the dielectric permittivity of the gold nanoparticles. We then describe the extensions of the MG model that we have used to calculate the effective permittivity of the nanocomposites. Finally, we explain how the HFs and the GNGs are parameterized within the RCWA approach.
We used two different MG models to compute the effective properties of the composites. The material is described as an ensemble of inclusions (the gold nanoparticles) randomly distributed, with a given volume filling fraction f, in a given host matrix (the polymer). The inclusions and the matrix are described with the help of their respective dielectric permittivities ϵ_{incl} and ϵ_m. In the visible range, the permittivity of the polymer can be assumed to be constant and equal to $\epsilon_m = n_{PVA}^2 = 2.25$. On the other hand, the permittivity of the inclusions strongly depends on the wavelength. The most common way to model the latter behavior is to use the Drude model [32] or the tabulated data measured for bulk gold [33]. The latter option is usually preferred as it offers the possibility to account for the inter-band electronic transitions that take place in gold for wavelengths below 450 nm [34]. Even if this approach has proven to be fairly reliable, it has been pointed out that it is not fully appropriate for describing the behavior of gold at the nano-scale, especially very small nanostructures. More precisely, when the size of the nanoparticles is reduced below the mean free path of the electrons, typically 40 nm in gold [35], the latter are strongly scattered by the nanoparticle surface, thus influencing their behavior. This effect, known as confinement [36], can be taken into account by introducing a damping term in the Drude model, depending on the nanoparticles radius R and a phenomenological parameter A. Based on this observation, it has been shown that very good agreement can be reached by modifying the tabulated data for bulk gold to take into account the effect of confinement. Consequently, the expression obtained [37] for the permittivity of nanometric metallic inclusions is given by

$$\epsilon_{incl} = \epsilon_{bulk} - \frac{\omega_p^2}{\omega^2 + i\omega\left(\gamma + A\frac{v_F}{R}\right)} + \frac{\omega_p^2}{\omega^2 + i\omega\gamma}. \qquad (1)$$

where ϵ_{bulk} is the tabulated permittivity of bulk gold, ω_p the plasmon pulsation of gold, γ a phenomenological damping coefficient, v_F the Fermi velocity and A a coefficient that is introduced for adjusting the effect of confinement. Various values of A can be found in the literature [38,39] and here we take $A = 1$ [40,41].

Eq. (1) is then used to describe the effective permittivity of a nanocomposite material according to the standard MG model, that will be referred to as MGc ('c' stands for 'confinement'). For a volume fraction f of inclusions, the effective permittivity can be calculated with the help of the following expression

Preprints (www.preprints.org) | NOT PEER-REVIEWED | Posted: 5 February 2018 doi:10.20944/preprints201802.0039.v1

Peer-reviewed version available at Materials 2018, 11, 351; doi:10.3390/ma11030351

$$\epsilon_{eff} = \epsilon_m + 3f\epsilon_m \frac{\epsilon_{incl} - \epsilon_m}{\epsilon_{incl} + 2\epsilon_m - f(\epsilon_{incl} - \epsilon_m)}. \qquad (2)$$

In fact, this model is only valid under the following conditions: (i) the concentration of the nanocomposites is small enough, *i.e.* if the volume fraction is typically less than 10% and (ii) the nanoparticle radius falls in the range of 1 to 25 nm. The second condition reflects the fact that the MG model does not explicitly account for the nanoparticle size. However, experimentally it turns out that the nanoparticle size, and more precisely the size distribution of the nanoparticles assembly, may greatly affect the plasmonic response. To tackle this issue, extensions of the MG model, based on the Mie theory have been proposed that take into account the effect of particle size. Among them, the Modified Mie-Maxwell-Garnett model (MMMG) also introduces the effect of the nanoparticles size distribution [37,41]. Consequently, we compared the MGc model with this theory, together with Eq. (1) accounting for the effect of confinement, and computed the effective permittivity of the gold nanocomposites. This model is referred to MMMGc and is given by

$$\frac{\epsilon_{eff} - \epsilon_m}{\epsilon_{eff} + 2\epsilon_m} = \frac{f}{\int_{R_{min}}^{R_{max}} R^3 g(R) dR} \int_{R_{min}}^{R_{max}} \alpha_{Mie}(R) g(R) dR, \qquad (2)$$

where , $g(R)$ is the nanoparticle size distribution, with R_{min} and R_{max} its lower and upper bounds. Next,

$$\alpha_{Mie}(R) = \frac{3i\lambda^3}{16\pi^2 {\epsilon_m}^{\frac{3}{2}}} a_1(R) \qquad (3)$$

is the nanoparticle polarizability with $a_1(R)$ being the first Mie (electric dipole) coefficient [42]. Note that here we ignore the (usually) weak magnetic contribution.

Now that we have dealt with the effective permittivity of the nanocomposite films, we then use the RCWA approach to model the gratings as a periodic distribution of nanostructures. The parameterization of the system is sketched in Fig. 3. We introduce the parameter h_1 as the thickness of the nanocomposite layer; it can be smaller than the total thickness of the film h_{tot}. In other words, the parameters h_1 determines the localization of the nanoparticles in the film thickness. Indeed, SEM measurements performed on the cross section of samples deposited on silicon wafers have shown that in some cases, the gold nanoparticles are located only in a thin layer on the polymer film surface (see Fig.S8, section B of the SM).
The HFs are defined as multilayer structures composed of the glass substrate, a layer of pure polymer (of thickness $h_{tot} - h_1$) and a layer of nanocomposite (of thickness h_1). The volume fraction f of inclusions in the nanocomposite layer is normalized to ensure the conservation of the total mass of gold.

In the case of GNGs, we use the same parameterization except that the nanocomposite layer is now regarded as a succession of very thin layers in order to reproduce the surface profile of the grating. The surface profiles are assumed to be perfectly sinusoidal with an amplitude h_G (see Fig. 3(b)), so that the total volume of the nanocomposite layer is the same as that of a flat film defined by the same value of h_1. Consequently, the normalization of the volume fraction is the same as for a HF.

Preprints (www.preprints.org) | NOT PEER-REVIEWED | Posted: 5 February 2018 doi:10.20944/preprints201802.0039.v1

Peer-reviewed version available at Materials 2018, 11, 351; doi:10.3390/ma11030351

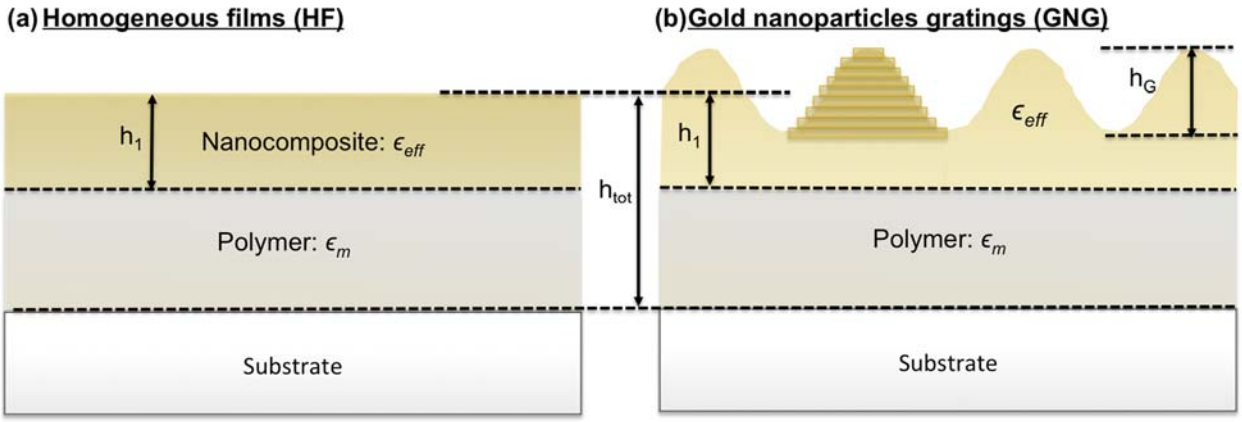

Figure 3: Parameterization of (a) the HFs and (b) the GNGs in the frame of the RCWA method.

Results and discussions

We are now ready to compare the experimental spectra with the results of our calculations. In order to validate our theoretical method, we used as benchmarks the HFs and GNGs previously described in Materials and Methods. The absorption spectra of these composite films are shown in Figs. 5 and 7. It should be underlined that the GNGs exhibit a novel plasmon-enhanced diffraction effect, that was previously reported in Ref. 32. This effect was defined as a resonant increase of the diffraction efficiency in the plasmon resonance domain, and can be quantified by drawing diffraction efficiency curves, see Fig. 7. The absorption and diffraction efficiency spectra have been simulated with the RCWA method, the dielectric permittivity of the composites being computed using either the MGc (Eq.2) or the MMMGc (Eq.3) model.

Let us first discuss the results for the HFs. For our simulations we use the experimental values for f (calculated from the Au/PVA ratio) and $h_1 = h_{tot} = 800$ nm, assuming that the nanoparticles are present in the total thickness of the films. Indeed, for HFs we found that h_1 has only a limited effect on the absorption spectra (additional information can be found in the SM, section B, Fig. S6). For the MMMGc model, the size distribution of the nanoparticles is required. In the case of the samples with 5%w and 10%w gold, experimental nanoparticles size distributions, built from the AFM images, were fitted with a lognormal distribution. The nanoparticles size distribution is built by measuring a large number of nanoparticles that are visible on the AFM images of the film's surface, for the samples at 5w% and 10w% (tip effects were estimated and taken into account when evaluating the nanoparticle size). Typical AFM images and the corresponding distributions for these samples are shown in Fig. 4. It was not possible to apply the same procedure to the HF at 3w% because no nanoparticles were visible on the film's surface from the AFM images. In the absence of experimental data, the size distribution was numerically optimized by fitting the absorption spectrum to obtain the best agreement between the simulated and the experimental data. For the MGc model, the effect of confinement, that depends explicitly on the nanoparticle size, was introduced by considering the mean value of the particle size distribution. Measured and simulated absorption spectra of the nanocomposites with Au/PVA ratio of 3w%, 5% and 10w% are given in Fig. 5.

Preprints (www.preprints.org) | NOT PEER-REVIEWED | Posted: 5 February 2018 doi:10.20944/preprints201802.0039.v1

Peer-reviewed version available at Materials 2018, 11, 351; doi:10.3390/ma11030351

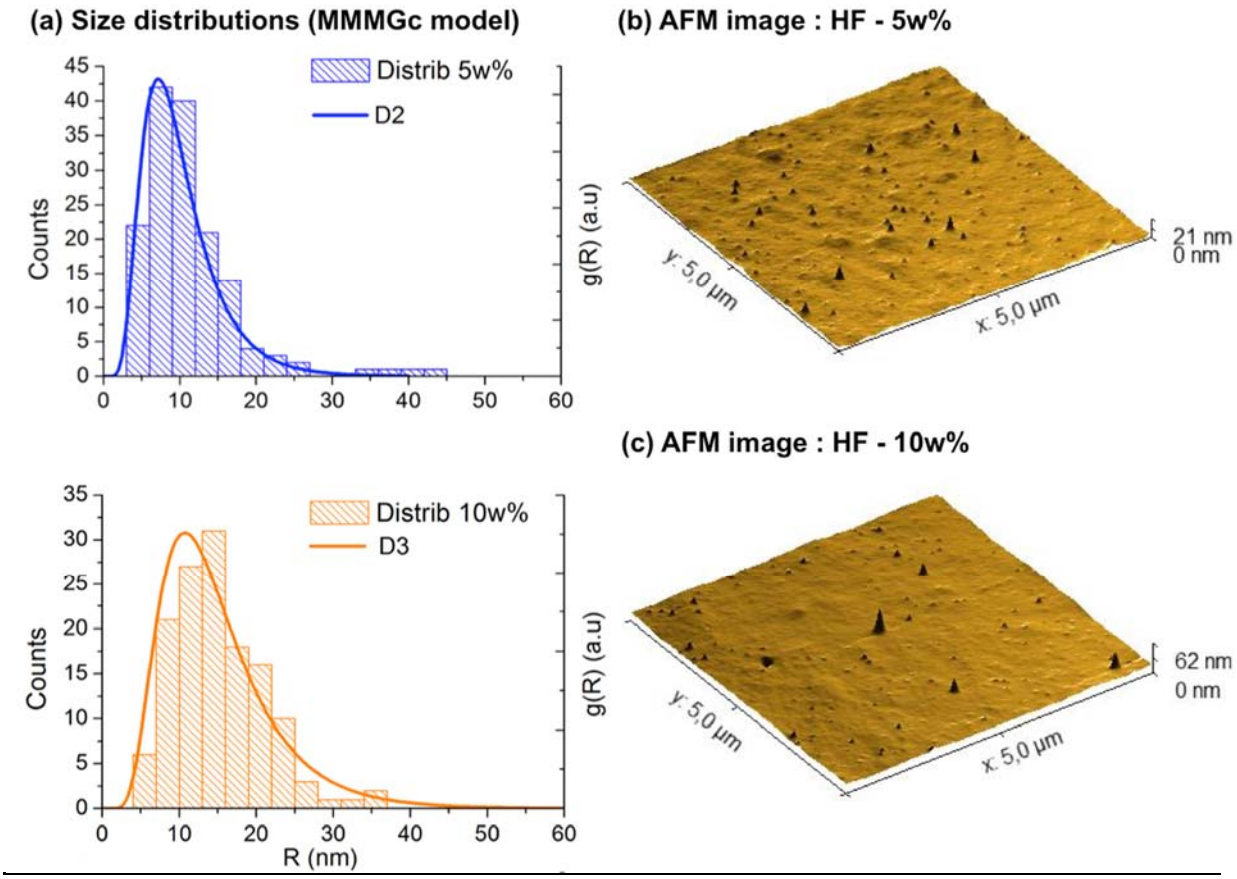

Figure 4: (a) Histogram and fitted size distribution of the HFs at 5w% and 10w%. (b) 3D view of typical AFM images of these samples.

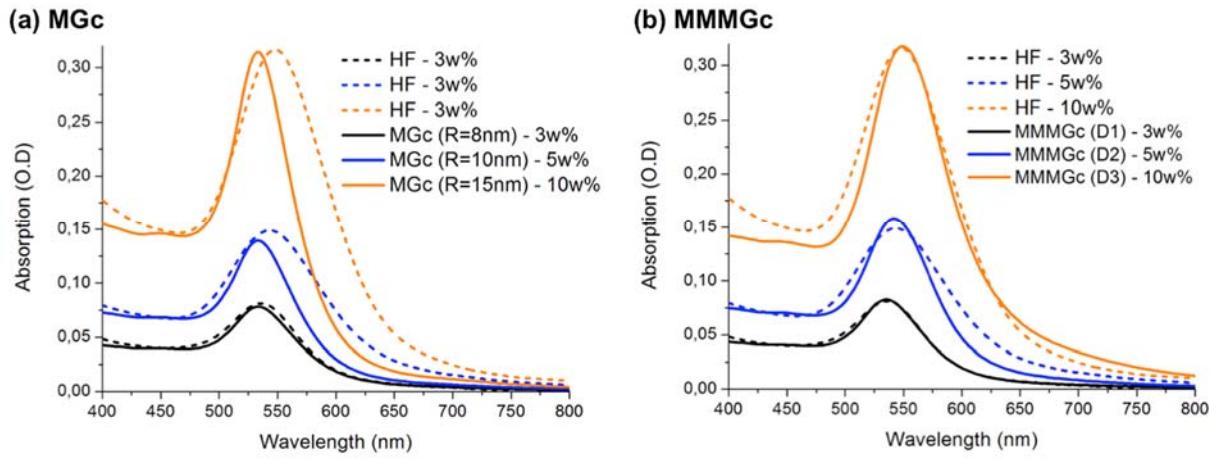

Figure 5: Comparison between the absorption spectra measured experimentally and the simulation using the MGc model and the MMMGc model.

The results show that the predictions of the MGc model are slightly blue-shifted compared to the experimental data. However, the introduction of the size distribution by using the MMMGc model allows obtaining a very good agreement between simulation and experiment. The size distribution used for the sample at 3w%, that is narrower than the ones at higher concentration, is given in the SM (Section B, Fig. S5). Finally, the good agreement that is observed in terms of plasmon resonance amplitude between simulations and

Preprints (www.preprints.org) | NOT PEER-REVIEWED | Posted: 5 February 2018 doi:10.20944/preprints201802.0039.v1

Peer-reviewed version available at Materials 2018, 11, 351; doi:10.3390/ma11030351

experiments indicates that the total amount of gold introduced in the system has been reduced to metallic state during the fabrication procedure.
In summary, for simple systems such as HFs, our approach renders fairly good results, but it also shows that it is necessary to take account of the nanoparticles size distribution in the calculation of the effective permittivity.

Next, we analyze the results for the GNGs. As before, the total thickness of the film, h_{tot}= 800 nm, is the same for all samples and we use values of the volume fraction f calculated from the experimental gold concentration. The gratings heights, inferred from the surface profiles measured by AFM (see Fig. 2(b)), are h_G= 25 nm, 65 nm and 80 nm, respectively for the samples with Au/PVA ratio of 3w%, 5w% and 10w%. In contrast with HFs, here we have found that the localization of nanoparticles in GNGs plays a crucial role, in particular in what regards the diffraction properties. Indeed, as the periodic surface modulation is only superficial ($h_G \approx h_{tot}/10$), the concentration of the nanoparticles in this region strongly affects the diffraction efficiency of the system. From the fabrication point of view, it is likely that the localization of gold occurs during the irradiation process. As the gold ions experience the light intensity gradient of the interference pattern, they migrate toward the bright fringes and are photo-reduced near the surface of the films [43]. This would explain why the localization is more pronounced in the case of GNGs than for HFs, for which the irradiation is homogenous (no gradient). As for HFs, the nanoparticle size distribution used in the MMMGc model has been determined from AFM images for the nanocomposites at 5w% and 10w% (see Fig. 6), and numerically optimized for the nanocomposite at 3w% (the final distribution is given in Fig. S5 of the SM). The values of h_1 and all other simulation parameters for the GNGs are summarized in the SM (Section B, Fig. S9).

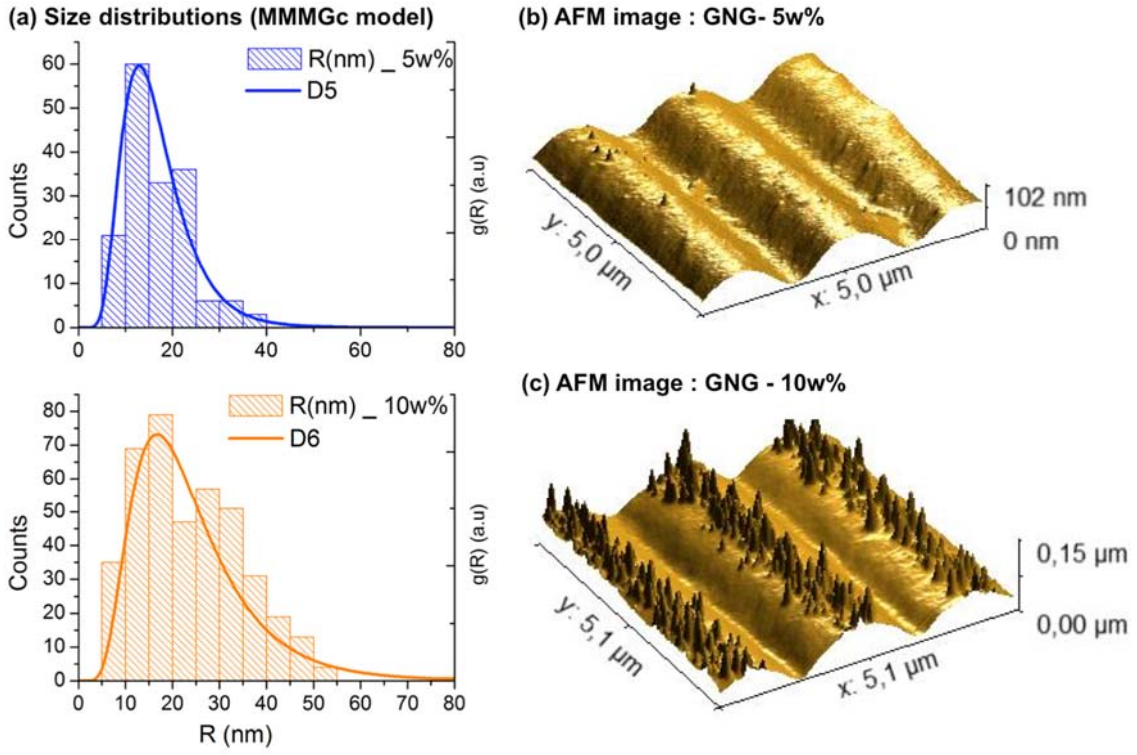

Figure 6: (a) Histograms and fitted size distributions of the GNGs at 5w% and 10w%. (b) 3D view of typical AFM images of these samples.

Preprints (www.preprints.org) | NOT PEER-REVIEWED | Posted: 5 February 2018 doi:10.20944/preprints201802.0039.v1

Peer-reviewed version available at Materials 2018, 11, 351; doi:10.3390/ma11030351

The experimental and simulated absorption and diffraction efficiency spectra are given in Fig. 7. The first important result that we would like to emphasize here is the fact that our approach correctly accounts for the optical behavior of the GNGs, and in particular enables to reproduce the plasmon-enhanced diffraction effect. Upon closely analyzing the details, we find that the simulations show that, except for low gold concentrations (3w%), the MGc model does not provide a quantitative agreement with the experimental data. Indeed, the simulated absorption curves for the samples with 5w% and 10 w% gold exhibit plasmon resonance profiles that are both narrower and blue-shifted as compared to the measured ones. The same conclusions can be drawn for the DE spectra which, even if they show the right tendency, do not allow for quantitative predictions. On the other hand, the results for the MMMGc model show that taking into account the particle size distribution qualitatively and quantitatively improve the results, in particular for the sample with 5w% gold. However, for 10w% gold, even if there is a better qualitative agreement between theory and experiment than for the MGc model, the discrepancies are still large in both absorption and diffraction efficiency spectra. In particular, with this approach, we cannot precisely predict the position of the plasmonic peaks at this concentration.

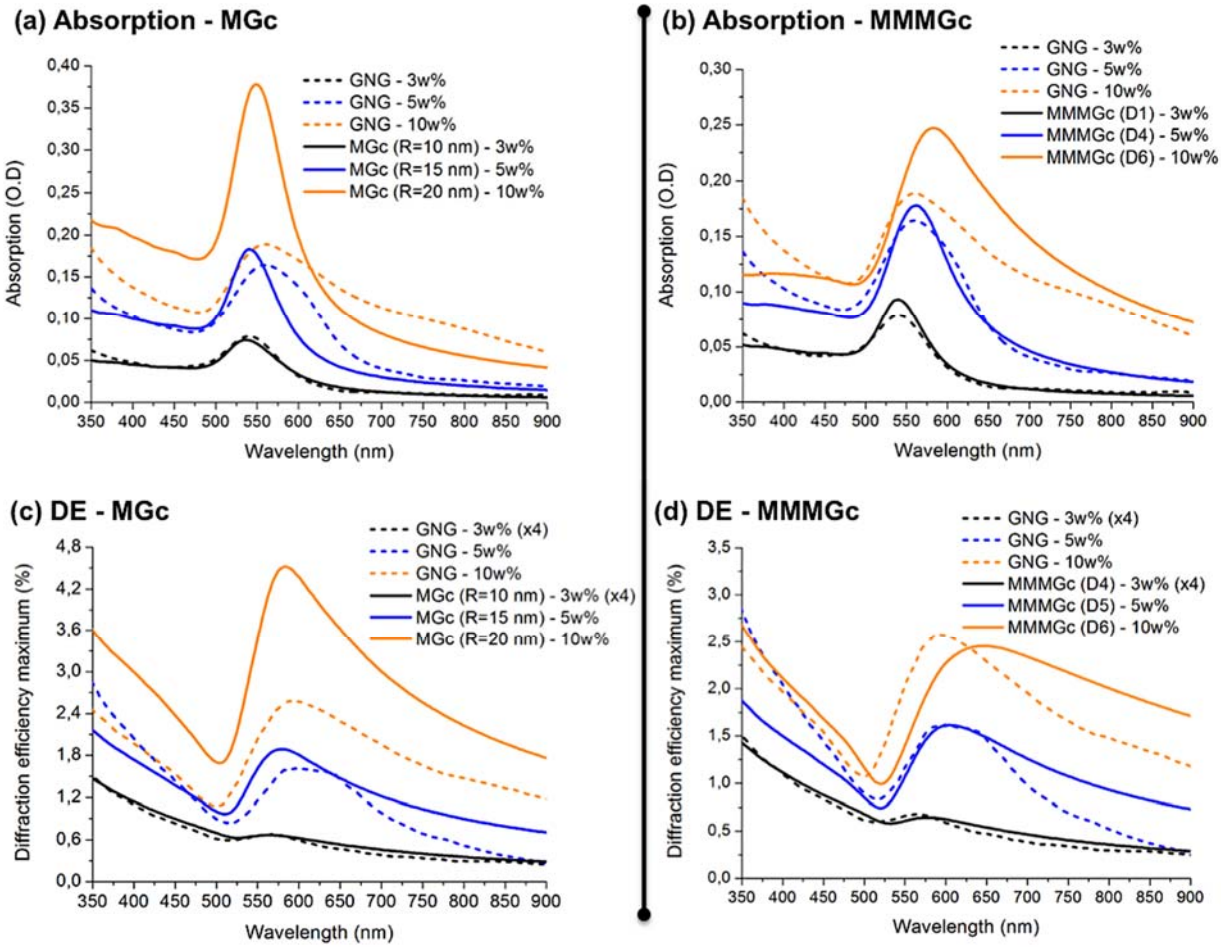

Figure 7: Comparison between the absorption spectra and the DE spectra measured experimentally and the simulated using the MGc model (left panel) and the MMMGc model (right panel).

Preprints (www.preprints.org) | NOT PEER-REVIEWED | Posted: 5 February 2018 doi:10.20944/preprints201802.0039.v1

Peer-reviewed version available at Materials 2018, 11, 351; doi:10.3390/ma11030351

The latter observation is, however, not quite surprising. Indeed, if we analyze the AFM images of the GNG at 10w% gold (see Fig. 6.(c)), we notice a very high density of nanoparticles at the grating crests emerging from the surface. This means that the nanoparticles are not fully embedded in the polymer matrix anymore, so that our simulations based on the effective medium approach are not really suitable for describing the system. For a better description of the emerging nanoparticles, we proposed a new parametrization of the system (M2) sketched in Fig. 8(a). First, we increase the grating height in order to include, at least partially, the emerging nanoparticles inside the simulated nanocomposite layer. This leads to an effective grating height h_G^{eff}. Second, since the nanoparticles are partly covered by polymer on one side and by air on the other, they experience a different environment, which may be characterized by a smaller value of the matrix permittivity. Numerical optimization leads to h_G^{eff} = 110 nm and ϵ_m =1.82 (*i.e.* n = 1.35 instead of 1.5). The results obtained with this new model (M2) are compared with the previous ones (model M1, h_G=80 nm, ϵ_m =2.25) in Fig. 8.(b) and (c).

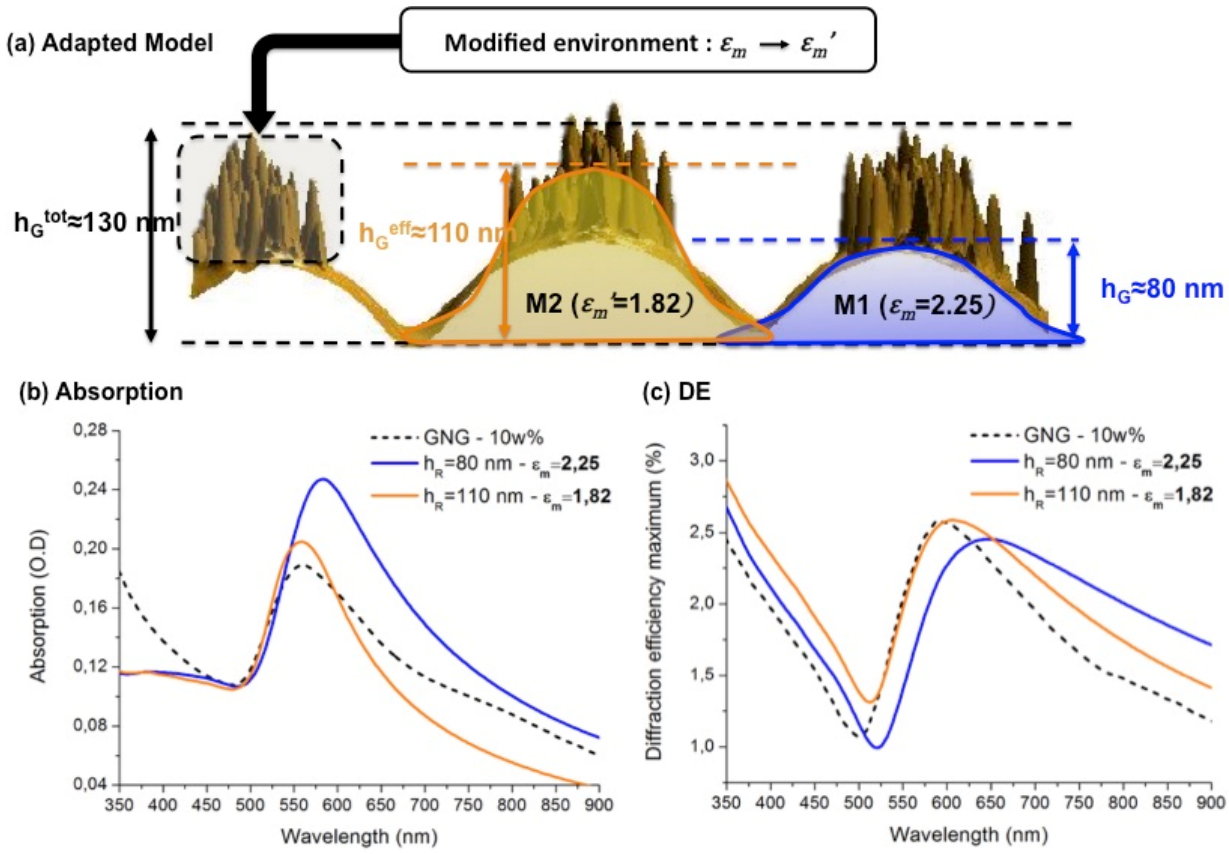

Figure 8: Specific consideration for the GNG at 10w%. (a) Parameters for the new modeling approach (M2) and the previous one (M1). (b) Absorption and (c) DE spectra of the GNG: comparison between the experimental data and the two models.

It is clear that the new set of parameters, which corresponds to a more plausible physical description of the GNG, improves the agreement between experiments and theory. We note in particular a better prediction regarding the resonances position and amplitude in both absorption and DE spectra. These two effects are mainly due to the change of environment (modified ϵ_m), since the plasmon resonance of nanoparticles becomes more blue-shifted and weaker in magnitude when the refractive index of their surrounding medium decreases.

Peer-reviewed version available at *Materials* **2018**, *11*, 351; doi:10.3390/ma11030351

It can be noticed that, even with this improved model, we cannot reproduce the shoulder appearing on the experimental spectra around 750-800 nm. Indeed, this feature, that appears only at high gold concentrations, may be attributed to plasmonic coupling between strongly packed nanoparticles [44]. Consequently, these effects cannot be described properly by the effective medium approach proposed here.

Conclusion

In conclusion, we have fabricated nanocomposites in the form of homogeneous films (HFs) and gold nanoparticle gratings (GNGs) by using an *in situ* synthesis approach under laser irradiation. We have measured and simulated both the absorption and the diffraction-efficiency spectra of these systems with a variable gold/polymer ratio. We have shown that the combination of RCWA and (extended) effective medium theories is a promising means for computing the optical properties of complex plasmonic systems. In particular, our simulations reproduce the previously observed effect of plasmon-enhanced diffraction in GNGs. More precisely, we have found that this approach not only renders fairly good results at low nanoparticle concentrations, but also applies in situations with higher concentrations. However, as the metallic fraction increases, it becomes necessary to take into account the nanoparticles size distribution through the MMMGc model to reach a quantitative agreement with experiment. Finally, we have speculated how the present model may be adapted so as to describe the specific configuration of GNGs at 10w%. This demonstrates the versatility of this approach and shows how it can be used for a better description of the physical behavior of structured plasmonic nanocomposites. We believe that this method, that is rather simple to implement and does not require substantial computational power, provides us with an efficient tool to study multi-scale plasmonic systems that cannot not be dealt using standard numerical approaches. For instance, it could be used to study the original optical properties that show up in metamaterials based on block-copolymer self-assembly [2,16,45]. In addition, for numerous nanocomposite systems, direct visualization of the inner structure of the material with the usual characterization techniques, such as SEM or TEM, can be quite challenging. In such a situation, our approach, and more especially the MMMGc model, could be used to investigate the nanoparticle size distribution and localization in the material upon fitting the experimental absorption spectra.

SUPPLEMENTARY MATERIALS

A. Experimental details

1. Sample fabrication

Fig.S1: Main steps of the fabrication method.

2. Optical measurements

Fig. S2: Absorption of the HFs and the GNGs with Au/PVA ratio of 3w%, 5w% and 10w%.

Fig. S3: Spectro-goniometer, setup used for the measurement of diffraction efficiency spectra.

Fig. S4: DE maps of the GNGs with Au/PVA ratio of (a) 3w%, (b) 5w% and (c) 10w% and the corresponding DE spectra (d).

Peer-reviewed version available at *Materials* **2018**, *11*, 351; doi:10.3390/ma11030351

B. Simulations

Fig. S5: Distributions obtained from numerical optimization for the HF and the GNG at 3w%.
Fig. S6: Effect of nanoparticles localization on the absorption spectra of a HF at 10w%.
Fig. S7: Parameters used for the simulation of HFs with Au/PVA ratio of 3w%, 5w% and 10 w%.
Fig. S8: SEM images of GNG cross-section showing the localization of the nanoparticle at the film surface.
Fig. S9: Parameters used for the simulation of GNGs with Au/PVA ratio of 3w%, 5w% and 10 w%.

FUNDING SOURCES

This project was supported by the laboratory PROMES (CNRS, UPR8521) and the University of Perpignan Via Domitia (UPVD).
This work was also supported by the Programme “Investissements d’avenir” (Investment for the Future) of the Agence Nationale de la Recherche (National Agency for Research) of the French State under award number ANR-10-LABX-22-01-SOLSTICE.

ACKNOWLEDGMENT

We would like to thank the PPCM team, and in particular Françoise Massines, for giving us access to their experimental facilities.
We thank Andreas Trügler for the rich discussion we had regarding the development and understanding of the extended Mawxell-Garnett models.

ABBREVIATIONS

Homogeneous Film (HF), Gold Nanoparticle Gratings (GNG), Polyvinyl alcohol (PVA), Atomic Force Microscopy (AFM), Scanning Electron Microscopy (SEM), Transmission Electron Microscopy (TEM), DE (Diffraction Efficiency).

REFERENCES

1. M. Hedayati, F. Faupel, and M. Elbahri, "Review of Plasmonic Nanocomposite Metamaterial Absorber," Materials (Basel). **7**, 1221–1248 (2014).
2. A. Malafronte, A. Capretti, G. P. Pepe, C. Forestiere, G. Miano, F. Auriemma, C. De Rosa, and R. Di Girolamo, "Simple Theoretical Considerations for Block-Copolymer-Based Plasmonic Metamaterials," in *Macromolecular Symposia* (2016), Vol. 359, pp. 72–78.
3. M. Stefik, S. Guldin, S. Vignolini, U. Wiesner, and U. Steiner, "Block copolymer self-assembly for nanophotonics," Chem. Soc. Rev. **44**, 5076–5091 (2015).
4. E. Stratakis and E. Kymakis, "Nanoparticle-based plasmonic organic photovoltaic devices," Mater. Today **16**, 133–146 (2013).
5. V. J. Babu, S. Vempati, S. Sundarrajan, M. Sireesha, and S. Ramakrishna, "Effective nanostructred morphologies for efficient hybrid solar cells," Sol. Energy **106**, 1–22 (2014).
6. C. Cocoyer, L. Rocha, C. Fiorini-Debuisschert, L. Sicot, D. Vaufrey, C. Sentein, B.

Geffroy, and P. Raimond, "Implementation of a submicrometer patterning technique in azopolymer films towards optimization of photovoltaic solar cells efficiency," Thin Solid Films **511**–**512**, 517–522 (2006).

7. A. Soum-Glaude, L. Di Giacomo, S. Quoizola, T. Laurent, and G. Flamant, "Selective Surfaces for Solar Thermal Energy Conversion in CSP: From Multilayers to Nanocomposites," in *Nanotechnology for Energy Sustainability* (Wiley-VCH Verlag GmbH & Co. KGaA, 2017), pp. 231–248.
8. R. Sellappan, M. G. Nielsen, F. González-Posada, P. C. K. Vesborg, I. Chorkendorff, and D. Chakarov, "Effects of plasmon excitation on photocatalytic activity of Ag/TiO 2 and Au/TiO2 nanocomposites," J. Catal. **307**, 214–221 (2013).
9. M. Wang, M. Ye, J. Iocozzia, C. Lin, and Z. Lin, "Plasmon-mediated solar energy conversion via photocatalysis in noble metal/semiconductor composites," Adv. Sci. **3**, 1600024 (2015).
10. X.-C. Ma, Y. Dai, L. Yu, and B.-B. Huang, "Energy transfer in plasmonic photocatalytic composites," Light Sci. Appl. **5**, (2016).
11. S. Mubeen, J. Lee, N. Singh, S. Krämer, G. D. Stucky, and M. Moskovits, "An autonomous photosynthetic device in which all charge carriers derive from surface plasmons.," Nat. Nanotechnol. **8**, 247–51 (2013).
12. P. A. DeSario, J. J. Pietron, D. E. DeVantier, T. H. Brintlinger, R. M. Stroud, and D. R. Rolison, "Plasmonic enhancement of visible-light water splitting with Au–TiO2 composite aerogels," Nanoscale **5**, 8073 (2013).
13. W. R. Erwin, A. Coppola, H. F. Zarick, P. Arora, K. J. Miller, and R. Bardhan, "Plasmon enhanced water splitting mediated by hybrid bimetallic Au–Ag core–shell nanostructures," Nanoscale **6**, 12626–12634 (2014).
14. J. F. Maguire, "Polymer Nanocomposites With Prescribed Morphology : Going Beyond Nanoparticle- Filled Polymers (Preprint)," Chem. Mater. **19**, 2736–2751 (2007).
15. M. K. Hedayati, F. Faupel, and M. Elbahri, "Review of plasmonic nanocomposite metamaterial absorber," Materials (Basel). **7**, 1221–1248 (2014).
16. X. Lu, D. P. Song, A. Ribbe, and J. J. Watkins, "Chiral Arrangements of Au Nanoparticles with Prescribed Handedness Templated by Helical Pores in Block Copolymer Films," Macromolecules **50**, 5293–5300 (2017).
17. W. Ye, R. Long, H. Huang, and Y. Xiong, "Plasmonic nanostructures in solar energy conversion," J. Mater. Chem. C **5**, 1008–1021 (2016).
18. T. J. Davis, D. E. Gómez, and A. Roberts, "Plasmonic circuits for manipulating optical information," Nanophotonics **6**, 543–559 (2017).
19. A. T. Juhl, J. D. Busbee, J. J. Koval, L. V Natarajan, V. P. Tondiglia, R. A. Vaia, T. J. Bunning, and P. V Braun, "Holographically directed assembly of polymer nanocomposites.," ACS Nano **4**, 5953–5961 (2010).
20. B. Gallinet, J. Butet, and O. J. F. Martin, "Numerical methods for nanophotonics: Standard problems and future challenges," Laser Photonics Rev. **9**, 577–603 (2015).
21. B. T. Draine and B. T., "The discrete-dipole approximation and its application to interstellar graphite grains," Astrophys. J. **333**, 848 (1988).
22. M. A. Yurkin and A. G. Hoekstra, "The discrete dipole approximation: An overview and recent developments," J. Quant. Spectrosc. Radiat. Transf. **106**, 558–589 (2007).
23. A. Taflove, A. Oskooi, and S. G. Johnson, *Advances in FDTD Computational Electrodynamics: Photonics and Nanotechnology* (2013).
24. A. Trügler, "Modeling the Optical Response of Metallic Nanoparticles," in (2016), pp. 101–127.
25. U. Hohenester and A. Trügler, "MNPBEM - A Matlab toolbox for the simulation of

plasmonic nanoparticles.," Comput. Phys. Commun. **183**, 370–381 (2012).

26. V. Myroshnychenko, J. Rodríguez-Fernández, I. Pastoriza-Santos, A. M. Funston, C. Novo, P. Mulvaney, L. M. Liz-Marzán, and F. J. García de Abajo, "Modelling the optical response of gold nanoparticles.," Chem. Soc. Rev. **37**, 1792–805 (2008).
27. T. C. Choy, *Effective Medium Theory: Principles and Applications* (2015).
28. V. A. Markel, "Introduction to the Maxwell Garnett approximation: tutorial," J. Opt. Soc. Am. A **33**, 1244 (2016).
29. K. Knop, "Rigorous diffraction theory for transmission phase gratings with deep rectangular grooves," J. Opt. Soc. Am. **68**, 1206 (1978).
30. L. Li, "Multilayer modal method for diffraction gratings of arbitrary profile, depth, and permittivity: addendum," J. Opt. Soc. Am. A **11**, 1685 (1994).
31. E. Nadal, N. Barros, H. Glénat, J. Laverdant, D. S. Schmool, and H. Kachkachi, "Plasmon-enhanced diffraction in nanoparticle gratings fabricated by in situ photo-reduction of gold chloride doped polymer thin films by laser interference patterning," J. Mater. Chem. C **5**, 3553–3560 (2017).
32. J. D. Jackson, *Classical Electrodynamics*, 3rd ed. (Wiley, 1999).
33. P. B. Johnson and R. W. Christy, "Optical Constants of the Noble Metals," Phys. Rev. B **6**, 4370–4379 (1972).
34. A. Derkachova, K. Kolwas, and I. Demchenko, "Dielectric Function for Gold in Plasmonics Applications: Size Dependence of Plasmon Resonance Frequencies and Damping Rates for Nanospheres," Plasmonics **11**, 941–951 (2016).
35. N. W. Ashcroft and N. D. Mermin, *Solid State Physics* (Holt, Rinehart and Winston, 1976).
36. J. Lermé, G. Celep, M. Broyer, E. Cottancin, M. Pellarin, A. Arbouet, D. Christofilos, C. Guillon, P. Langot, N. Del Fatti, and F. Vallée, "Effects of confinement on the electron and lattice dynamics in metal nanoparticles," in *European Physical Journal D* (EDP Sciences, 2005), Vol. 34, pp. 199–204.
37. R. Ruppin, "Evaluation of extended Maxwell-Garnett theories," Opt. Commun. **182**, 273–279 (2000).
38. H. Havel, S. Fritz, A. Hilger, U. Kreibig, and M. Vollmer, "Width of cluster plasmon resonances: Bulk dielectric functions and chemical interface damping," Phys. Rev. B **48**, 18178–18188 (1993).
39. M. Hu, C. Novo, A. Funston, H. Wang, H. Staleva, S. Zou, P. Mulvaney, Y. Xia, and G. V Hartland, "Dark-field microscopy studies of single metal nanoparticles: understanding the factors that influence the linewidth of the localized surface plasmon resonance," J. Mater. Chem. **18**, 1949–1960 (2008).
40. S. Berciaud, L. Cognet, P. Tamarat, and B. Lounis, "Observation of intrinsic size effects in the optical response of individual gold nanoparticles," Nano Lett. **5**, 515–518 (2005).
41. Y. Battie, A. Resano-Garcia, N. Chaoui, Y. Zhang, and A. En Naciri, "Extended Maxwell-Garnett-Mie formulation applied to size dispersion of metallic nanoparticles embedded in host liquid matrix," J. Chem. Phys. **140**, (2014).
42. G. Mie, "Beiträge zur Optik trüber Medien, speziell kolloidaler Metallösungen," Ann. Phys. **330**, 377–445 (1908).
43. E. Yilmaz, G. Ertas, E. Bengu, and S. Suzer, "Photopatterning of PMMA Films with Gold Nanoparticles: Diffusion of Au Cl 4 - Ions," J. Phys. Chem. C **114**, 18401–18406 (2010).
44. S. K. Ghosh and T. Pal, "Interparticle coupling effect on the surface plasmon resonance of gold nanoparticles: from theory to applications.," Chem. Rev. **107**, 4797–862 (2007).

45. Y. H. Lee, T. K. Lee, I. Song, H. Yu, J. Lee, H. Ko, S. K. Kwak, and J. H. Oh, "Boosting the Performance of Organic Optoelectronic Devices Using Multiple-Patterned Plasmonic Nanostructures," Adv. Mater. 4976–4982 (2016).